Evaluation of liquefaction probability of earth-fill dam over next 50 years using geostatistical method based on CPTU

Kazunari Imaide
University of Texas at Austin, Austin, United States, ev422304@s.okayama-u.ac.jp

Shin-ichi Nishimura[1], Toshifumi Shibata[2], Takayuki Shuku[3] (from same institution)
Okayama University, Okayama, Japan, theg1786@okayama-u.ac.jp[1], tshibata@cc.okayama-u.ac.jp[2], shuku@cc.okayama-u.ac.jp[3]

ABSTRACT: In this paper, the spatial distribution of the liquefaction probability inside the studied dam was calculated from CPTUs including conversion errors and the spatial variability of the soil parameters. In addition, based on the seismic hazard at the studied site and the fragility, the spatial average of the liquefaction probability over the next 50 years was evaluated. Although the CPTU is often preferable for identifying the liquefaction probability, the CPTU is still not widely used in Japan. Therefore, the focus will be placed here on the SPT *N*-value and the fines content, F_c, because the majority of the accumulated site characterization data in Japan consists of SPT *N*-values and F_c. Utilizing the conditional simulation, the spatial distribution of the expected values for F_c and N_{SPT} inside the dam were calculated with high spatial resolution. Based on the results of the simulation the scale of the weak areas and the spatial continuity of the soil profile of the dam were clarified.

Keywords: liquefaction; cone penetration test; seismic hazard; geostatistics; spatial variability

1. INTRODUCTION

There are many earth-fill dams for agriculture in Japan. Most of them were constructed 150-500 years ago and have become old and decrepit. In addition, over the next 30 years, the probability of an earthquake occurring in the Nankai Trough is reported to be about 70%. And it is predicted that the magnitude of this earthquake will be as large as 9.0. Such an earthquake would affect a wide area from western to central Japan. In the 2011 off the Pacific coast of Tohoku Earthquake, the failure of the Fujinuma Dam was found to have been caused by liquefaction inside the dam (e.g., Tatsuoka et al., 2017; Ono et al., 2011). Since then, the design guidelines for earth-fill dams for irrigation have demanded an evaluation of the probable liquefaction damage (Ministry of Agriculture, Forestry, and Fisheries of Japan, 2015). For the above-mentioned reasons and to prevent the failure of dams against great earthquakes, the efficient improvement of the dams is required within a limited time and with a limited budget. Evaluating and comparing the seismic risk of various dams enables a quantitative prioritization of the dams such that a decision can be made on which dams among many are to be improved. In general, the seismic risk is expressed by the multiplication of the failure probability by the cost of failure. Therefore, a new procedure is proposed here for evaluating the liquefaction probability of a dam against a potential Nankai Trough earthquake.

The novelty of the proposed work comes from the statistical modeling of the SPT (Standard penetration test) *N*-value and F_c based on the CPTUs (Cone penetration tests), including the conversion of the measured values from the CPTUs into the SPT *N*-value and F_c for evaluating the liquefaction probability. A unique feature of the proposed work is its potential capability to take into account the accumulated site characterization data, such as the SPT *N*-value and F_c, adjacent to the studied site. An illustrative example assessing the liquefaction probability of an earth-fill dam in Japan is presented to demonstrate the capability of the proposed method.

2. SITE INVESTIGATION

An earth-fill dam in Hiroshima Prefecture, Japan is analyzed. The earth-fill dam is one of the dams for which there is a fear of liquefaction damage should a Nankai Trough earthquake occur. In Japan, to design countermeasures against the liquefaction of an earth-fill dam, the *N*-value obtained from the SPT is generally used. In the Japanese design code for earth-fill dams for irrigation, the liquefaction resistance factor F_L method, originally based on the study of Iwasaki et al. (1984), is used. In Iwasaki's method, the *N*-value and fines content F_c are utilized to calculate F_L. Therefore, the measured values from CPTUs on the dam are firstly converted into the soil behavior type index, I_c, proposed by Robertson and Wride (1998). Then, I_c is used to obtain the *N*-value and F_c by utilizing the conversion formulas which were originally proposed by Suzuki et al. (2003).

The CPTU is employed to obtain several soil parameters, such as corrected cone resistance q_t, measured sleeve friction f_s, and pore water pressure u in short intervals. CPTUs were conducted at 15 points at the top of the dam at intervals of 2 m along the crest, as shown in Figure 1. The geological cross section at the studied site is given in Figure 2.

The CPTU results can be used to estimate the ground composition. To conduct the soil classification based on the CPTUs, the soil behavior type index, I_c, was proposed, as seen in Eq. (1) (Robertson and Wride, 1998).

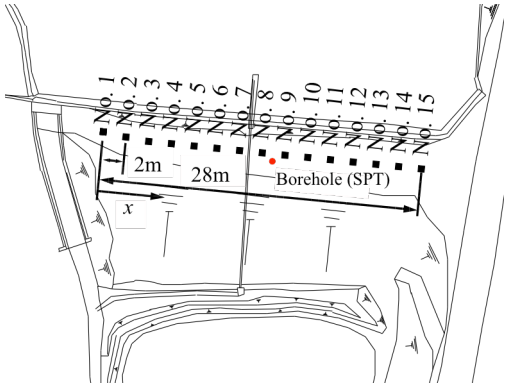

Figure 1. Plan view of dam and testing points of CPTs and SPT.

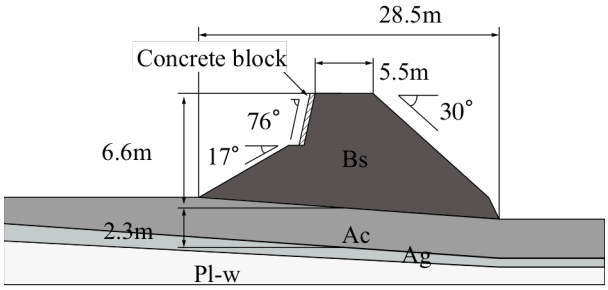

Bs : Backfill sand Ag : Alluvial gravel

Ac : Alluvial clay Pl-w : Weathered slate

Figure 2. Geological cross section of dam.

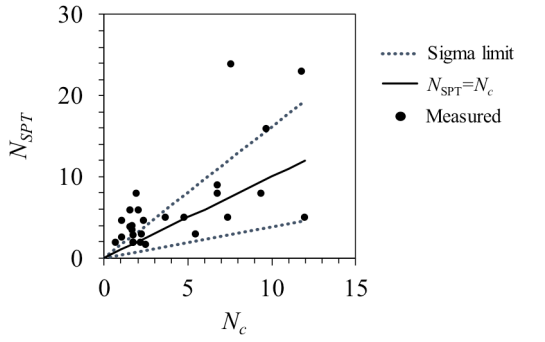

Figure 3. Comparison of N_c and N_{SPT}. This figure was derived from data on earth-fill dams.

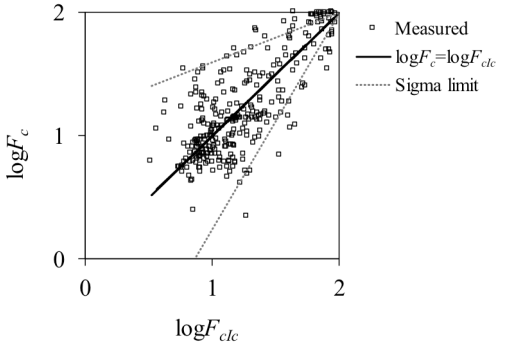

Figure 4. Comparison of logF_{clc} and logF_c. This figure was derived from data included in Suzuki et al. (2003).

I_c includes two normalized parameters, Q and F, given by Eqs. (2) and (3) (Robertson, 1990), respectively.

$$I_c = \left[\left(3.47 - \log Q\right)^2 + \left(1.22 + \log F\right)^2\right]^{0.5} \quad (1)$$

$$Q = \left(q_t - \sigma_{v0}\right)/\sigma'_{v0} \quad (2)$$

$$F = \left[f_s/\left(q_t - \sigma_{v0}\right)\right] \times 100\% \quad (3)$$

where Q is the normalized CPT penetration resistance, F is the normalized friction ratio (%), q_t is the corrected cone resistance (kPa), f_s is the measured sleeve friction (kPa), and σ_{v0} and σ'_{v0} are the total and the effective overburden stresses (kPa), respectively. Corrected cone resistance q_t and measured sleeve friction f_s are directly measured values in the CPTUs.

Based on I_c and q_t, obtained from the CPTUs, the CPTU N-value, N_c, and the fines content, F_{cIc}, obtained from I_c, can be estimated by the following equations. Eq. (4) was proposed by Suzuki et al. (2003), while Eq. (5) was derived from the data included in Suzuki et al. (2003).

$$\begin{aligned} N_c &= 0.341 I_c^{1.94}\left(q_t - 0.2\right)^{\left(1.34 - 0.0927 I_c\right)} && \left(q_t > 0.2\text{MPa}\right) \\ N_c &= 0 && \left(q_t \le 0.2\text{MPa}\right) \end{aligned} \quad (4)$$

$$F_{clc} = 1.0 I_c^{3.2293} \cdot 10^{0.3024} \quad (\%) \quad (5)$$

Since the above-mentioned conversion formulas are based on experimental data, conversion errors could be included. However, in Eqs. (4) and (5), the conversion errors are not explicitly considered. Thus, the conversion errors are quantified based on measured data.

Based on the idea of Suzuki et al. (2003), that N_c is equivalent to N_{SPT}, Fig. 3 shows the relationship between N_c and N_{SPT} included in the data of earth-fill dams. As a result, N_c is converted into N_{SPT} by the following equation considering the conversion error:

$$N_{SPT} = N_c\left(1 + 0.62\varepsilon_i\right) \quad (6)$$

where error term ε_i is assumed to obey standard normal distribution N (0,1). In Eq. (6), N_c is assumed to be equal to N_{SPT}, and the quantity of the conversion error is given by the coefficient of variation calculated from the values of the ratio of N_{SPT} to N_c. In addition, the conversion error is proportional to N_c and corresponds to 0 when $N_c = 0$.

The relationship between fines content logF_{cIc}, obtained from I_c, and the proper fines content, logF_c is given in Fig. 4. logF_{cIc} is converted into logF_c by the following equation considering the conversion error:

$$\log F_c = 2 - \left(2 - \log F_{clc}\right)\left(1 + 0.598\varepsilon_j\right) \quad (7)$$

where error term ε_j is assumed to obey standard normal distribution N (0,1). logF_{cIc} is assumed to be equal to logF_c, and the quantity of the conversion error is given by the coefficient of variation calculated from the values of the ratio of logF_{cIc} to logF_c. In addition, the conversion error is in inverse proportion to logF_c and corresponds to 0 when logF_c = 2.

3. STATISTICAL MODEL IDENTIFICATION OF STUDIED DAM

A Statistical models of soil parameters are useful for visualizing the spatial variability of the soil parameters. This is because the soil parameters for the points where test results do not exist can be estimated using the statistical models. The statistical models of the CPTU results are determined based on a geostatistical method (Journel and Huijbregts, 1978) and random field theory.

Table 1 Statistical models of logN_c and logF_{clc} estimated by MAIC.

	Mean function	Covariance function (i, j=1, 2, …, M)
logN_c	$m = 0.370 - 0.012x - 0.030z$ $+0.001x^2 + 0.005z^2 - 0.001xz$	$\mathbf{C} = [C_{ij}] = 0.246^2 \exp\left(-\lvert x_i - x_j\rvert/0.01 - \lvert z_i - z_j\rvert/0.28\right)$ $(i \neq j)$ $\mathbf{C} = 0.246^2$ $(i = j)$
logF_{clc}	$m = 0.874 + 0.021x + 0.217z$ $-0.001x^2 - 0.019z^2 - 0.0001xz$	$\mathbf{C} = [C_{ij}] = 0.123^2 \cdot 0.688 \cdot \exp\left(-\lvert x_i - x_j\rvert/2.28 - \lvert z_i - z_j\rvert/1.10\right)$ $(i \neq j)$ $\mathbf{C} = 0.123^2$ $(i = j)$

m : Mean function, x : Horizontal coordinate (m), z : Depth (m)

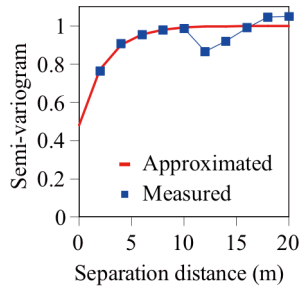

(a) Semi-variograms of horizontal direction.

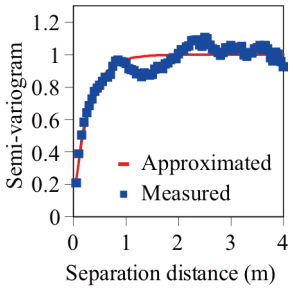

(b) Semi-variograms of depth direction.

Figure 5. Semi-variograms and approximation function of logN_c.

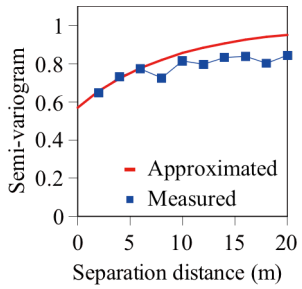

(a) Semi-variograms of horizontal direction.

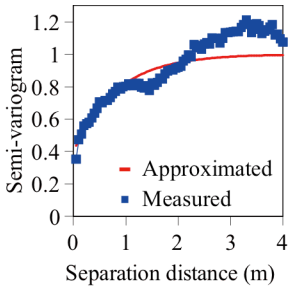

(b) Semi-variograms of depth direction.

Figure 6. Semi-variograms and approximation function of logF_{clc}.

Although the soil parameters utilized to calculate the liquefaction probability have spatial variability, the variability can be introduced into the statistical models explicitly. Since the densely obtained data on the dam by CPTUs are converted into N-values and fines content F_c, a large amount of N-values and F_c data can be utilized for statistical model identification.

The representative variable for soil parameter s is defined by Eq. (8) as the function of location X = (x, z). It is assumed that variable s is expressed as the sum of trend function m and fluctuation component U, which is a normal random variable.

$$s(\mathbf{X}) = m(\mathbf{X}) + U(\mathbf{X}) \tag{8}$$

The hypothesis is commonly used to model the soil parameters (e.g., Vanmarcke, 1983; Phoon and Kulhawy, 1999). Herein, based on the method of maximum likelihood (MLE), the statistical models are determined for CPTU N-value logN_c and fines content logF_{clc}. The detailed procedure for the statistical model identification is described in Nishimura (2016). In the model identification based on MLE, the Akaike's information criterion (AIC) is used. The mean functions, the standard deviations, and the covariance functions of logN_c and logF_{clc} are determined by the minimum Akaike's information criterion (MAIC) procedure (Akaike, 1974). The covariance function is assumed to be of an exponential type and composed of several parameters, such as the standard deviation, the correlation distance of horizontal and depth directions, and the nugget effect parameter.

Table 1 presents the mean function and the covariance function of logN_c and logF_{clc} estimated by MAIC. As shown in Table 1, lateral correlation distance l_x in the model of logN_c, obtained by MAIC, is not reasonable, because the value is identified as being the lower boundary value of 0.01 m. In the MAIC, the correlation structure of the multi-points distributed multi-dimensionally are evaluated simultaneously, and this procedure sometimes creates difficulty. On the other hand, since calculating the semi-variogram (Journel and Huijbregts, 1976) is the method for identifying the correlation distance one-dimensionally, it is easier to use the semi-variogram than the MAIC for finding the correlation distance. The semi-variograms of horizontal direction l_x and depth direction l_z are defined by the following equations, respectively:

$$\gamma_x\left(\lvert x_i - x_j\rvert\right) = \frac{1}{2D_x}\sum_{k=1}^{D_x}\left[U(x_k) - U\left(x_k + \lvert x_i - x_j\rvert\right)\right]^2$$
$$\gamma_z\left(\lvert z_i - z_j\rvert\right) = \frac{1}{2D_z}\sum_{k=1}^{D_z}\left[U(z_k) - U\left(z_k + \lvert z_i - z_j\rvert\right)\right]^2 \tag{9}$$

where D_x and D_z denote the number of combinations of $U(x_k) - U\left(x_k + \lvert x_i - x_j\rvert\right)$ and $U(z_k) - U\left(z_k + \lvert z_i - z_j\rvert\right)$, respectively, in which $\lvert x_i - x_j\rvert$ and $\lvert z_i - z_j\rvert$ mean the separation distances in the horizontal and vertical

Table 2 Constants of covariance functions of logN_c and logF_{cIc} determined by semi-variograms.

	C_0	C_1	C.L. (m)
logN_c	C_{0x}=0.48, C_{0z}=0.08	C_{1x}=0.52, C_{1z}=0.92	l_x=2.42, l_z=0.29
logF_{cIc}	C_{0x}=0.57, C_{0z}=0.40	C_{1x}=0.43, C_{1z}=0.60	l_x=9.17, l_z=0.82

C.L. : Correlation length

directions. $U(x_k)$ is $|x_i - x_j|$ away from $U\left(x_k + |x_i - x_j|\right)$ at the same depth, and similarly, $U(z_k)$ is $|z_i - z_j|$ away from $U\left(z_k + |z_i - z_j|\right)$ at the same horizontal coordinate. Figs. 5 and 6 show the semi-variograms of logN_c and logF_{cIc} for the horizontal and depth directions, respectively, of the dam. In the calculation of semi-variograms, the measured values are assumed to be standard normal distribution N (0, 1). For example, logN_c is standardized as $f = (\log N_c - m)/\sigma$ to remove the trend where m is the mean value and σ is the standard deviation; they are obtained from MAIC. In addition, in order to set the f values to be N (0, 1) with certainty, the following equation is used here:

$$Y = \Phi^{-1}\left[F(f)\right] \tag{10}$$

where F is the cumulative distribution function of f and Φ is the standard normal distribution function. To identify the geostatistical parameters of a standardized value Y, the approximation curve is simply modeled by an exponential function as the following equations:

$$\begin{aligned}
&\gamma_x\left(|x_i - x_j|\right) = C_{0x} + C_{1x}\left[1 - \exp\left(-|x_i - x_j|/l_x\right)\right] \quad (i \neq j)\\
&\gamma_z\left(|z_i - z_j|\right) = C_{0z} + C_{1z}\left[1 - \exp\left(-|z_i - z_j|/l_z\right)\right] \quad (i \neq j)\\
&\gamma_x(0) = \gamma_z(0) = 0
\end{aligned} \tag{11}$$

where, C_{0x} and C_{0z} are the parameters used for the nugget effect in the x and z directions, respectively, while C_{1x} and C_{1z} are the parameters used to express the shape of the semi-variogram functions. Based on the semi-variograms of the x and z directions, the covariance matrix $\mathbf{C}$ composed of the standardized values is assumed to have the following form:

$$\begin{aligned}
&\mathbf{C} = \left[C_{ij}\right] = N_e\sigma^2 \exp\left(-\frac{|x_i - x_j|}{l_x} - \frac{|z_i - z_j|}{l_z}\right) \quad (i \neq j)\\
&N_e = C_{1x}C_{1z} \quad \left(|x_i - x_j| \neq 0, |z_i - z_j| \neq 0\right)\\
&N_e = C_{1x} \quad \left(|x_i - x_j| \neq 0, |z_i - z_j| = 0\right)\\
&N_e = C_{1z} \quad \left(|x_i - x_j| = 0, |z_i - z_j| \neq 0\right)\\
&\left[C_{ij}\right] = \sigma^2 \quad (i = j)
\end{aligned} \tag{12}$$

As shown in Figs. 5 and 6, the approximation curves roughly correspond to the observed values. These approximation curves are derived by the least squares method, and finally, parameters C_{0x}, C_{1x}, C_{0z}, C_{1z}, l_x, and l_z are determined. The separation distances of the data, $\Delta x = |x_i - x_j|$ and $\Delta z = |z_i - z_j|$, are less than 6 m in the horizontal direction and less than 0.9 m in the depth direction, and are applied to identify the approximate functions, since the accuracy of the semi-variograms is high within the range of small values for lx and lz. Within the ranges of 10 m for the horizontal direction and 1 m for the vertical direction, the exponential correlation function simulates the actual correlations very well. For long separation distances, however, the variogram value should converge to 1.0 and the exponential function is appropriate. Table 2 shows the constants determined by the semi-variograms. The lateral correlation distance obtained from the semi-variograms is about 10 times that of the vertical one. The identified correlation distances are supposed to be reasonable, because this relationship agrees with the published values (Nishimura, 2007; Phoon and Kulhawy, 1999).

4. INTERPOLATION OF MEASURED VALUE OF CPTUs

Since the data measured by the CPTUs are point estimation values, the interpolation of these values is required for visualizing the spatial variability of the soil parameters. Thus, the geostatistical software library GSLIB (Deutsch and Journel, 1992) is used as a conditional simulation tool. In the conditional simulation, the realizations of the simulation are based on the statistical models of the soil parameters which are characterized by their first two moments and their covariance function. The realizations generated by the simulation are conditioned by the measured data, and the values of the realizations coincide with the measured values at the measuring points.

Utilizing the simulation tool, the cross section of the studied dam along the embankment axis is analyzed. The cross section is meshed into several grids at intervals of 1 m in the horizontal direction and 0.05 m in the depth direction. The grid spacing is selected such that it corresponds to the intervals of the CPTU data. The Monte Carlo method is repeated 2000 times to evaluate the spatial distribution of the expected values for N_{SPT} and F_c at the grid points. In addition, the validity of the interpolated values calculated from the conditional simulation was examined, and the results have been published in Imaide et al. (2018) and Imaide et al. (2019).

The statistical models for logN_c and logF_{cIc}, introduced into the simulation, are summarized in Table 3. In this table, the mean functions and the standard deviations are derived from MAIC, and the covariance functions are determined by the semi-variograms. The covariance function is assumed to be an exponential type of function.

Figs. 7 and 8 present the spatial distributions of the statistical values inside the dam derived from the conditional simulation. Figs. 7(a) and 8(a) correspond to the spatial distributions of the expected values for F_c and N_{SPT}, Figs. 7(b) and 8(b) correspond to the spatial distributions of the standard deviations for F_c and N_{SPT}, and Figs. 7(c) and 8(c) correspond to the spatial

Table 3 Statistical models for logN_c and logF_{clc} introduced into the simulation.

	Mean function	S.D.
logN_c	$m = 0.370 - 0.012x - 0.030z + 0.001x^2 + 0.005z^2 - 0.001xz$	σ=0.246
logF_{clc}	$m = 0.874 + 0.021x + 0.217z - 0.001x^2 - 0.019z^2 - 0.0001xz$	σ=0.123
	Covariance function (i, j=1, 2, …, M)	
logN_c	$\mathbf{C} = [C_{ij}] = \sigma^2 \cdot N_e \cdot \exp\left(-\lvert x_i - x_j\rvert/2.42 - \lvert z_i - z_j\rvert/0.29\right)\ (i \neq j)$	
	$N_e = 0.475\ \left(\lvert x_i - x_j\rvert \neq 0,\ \lvert z_i - z_j\rvert \neq 0\right)$	
	$N_e = 0.519\ \left(\lvert x_i - x_j\rvert \neq 0,\ \lvert z_i - z_j\rvert = 0\right)$	
	$N_e = 0.917\ \left(\lvert x_i - x_j\rvert = 0,\ \lvert z_i - z_j\rvert \neq 0\right)$	
	$\mathbf{C} = 0.246^2\ (i = j)$	
logF_{clc}	$\mathbf{C} = [C_{ij}] = \sigma^2 \cdot N_e \cdot \exp\left(-\lvert x_i - x_j\rvert/9.17 - \lvert z_i - z_j\rvert/0.82\right)\ (i \neq j)$	
	$N_e = 0.256\ \left(\lvert x_i - x_j\rvert \neq 0,\ \lvert z_i - z_j\rvert \neq 0\right)$	
	$N_e = 0.429\ \left(\lvert x_i - x_j\rvert \neq 0,\ \lvert z_i - z_j\rvert = 0\right)$	
	$N_e = 0.598\ \left(\lvert x_i - x_j\rvert = 0,\ \lvert z_i - z_j\rvert \neq 0\right)$	
	$\mathbf{C} = 0.123^2\ (i = j)$	

m : Mean function, S.D. : Standard deviation, x : Horizontal coordinate (m), z : Depth (m),
M : Number of test points, N_e : Nugget effect.

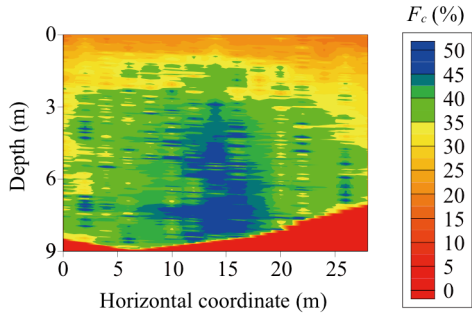

(a) Expected value (F_c)

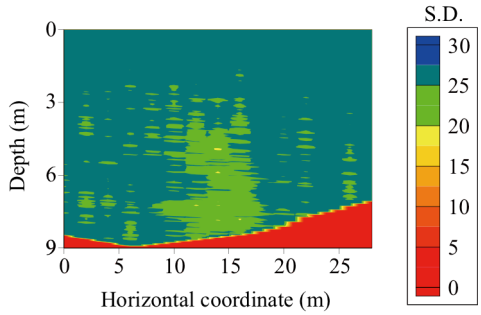

(b) Standard deviation (F_c)

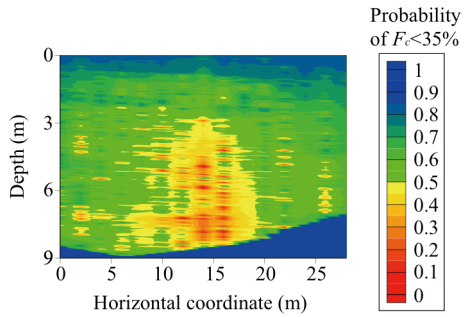

(c) Probability of F_c <35%

Figure 7. Spatial distribution of statistical values of F_c.

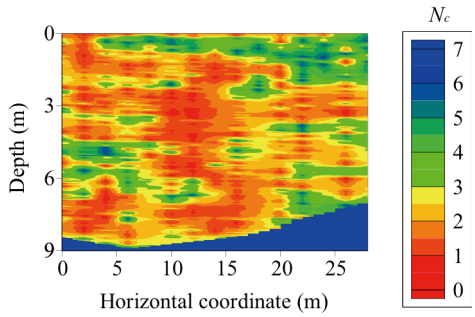

(a) Expected value (N_{SPT})

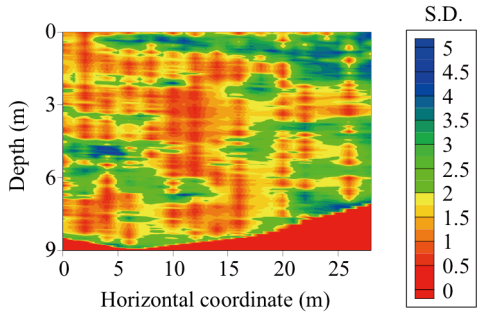

(b) Standard deviation (N_{SPT})

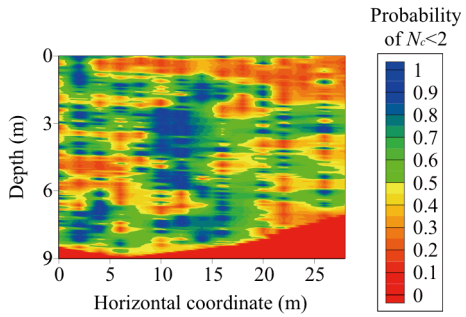

(c) Probability of N_{SPT} <2

Figure 8. Spatial distribution of statistical values of N_{SPT}.

distributions of the probability of F_c<35% and N_{SPT}<2, respectively.

According to Figure (a), the soil which comprises about 35-40% F_c is distributed in the dominant area of the dam. The soil profile for this area is categorized as

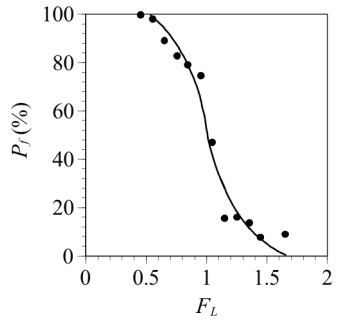

Figure 9. Relationship between liquefaction probability P_f and liquefaction resistance factor F_L (Relationship was derived from data included in Iwasaki et al., 1984).

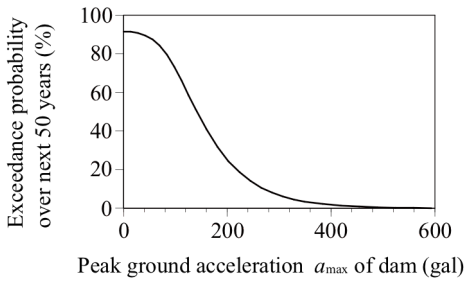

Figure 10. Seismic hazard curve of Nankai Trough earthquake of studied dam.

intermediate soil; it consists of sandy and fine materials. The area of x = 10-17 m and z = 3-9 m has a relatively high F_c (about 50%), because this area is located above the sluiceway inside the dam. Figure (b) shows the spatial distribution of the standard deviation of F_c, including the conversion error given in Eq. (7). Since the conversion error is considered, the standard deviation is large in the dominant area inside the dam, and the value is up to about 30%. In Figure (c), the probability of F_c<35% is more than 0.5 in the dominant area inside the dam, because the standard deviation is large.

According to Figure (a), the overall N-value inside the dam is relatively small. In particular, there are weak areas around x = 0-28 m and z = 3 m and x = 10-17 m and z = 3-9 m. Figure (b) shows the spatial distribution of the standard deviation of N_{SPT}, including the conversion error, as shown in Eq. (6). The standard deviations are relatively small at the test points where the expected values are small. Based on Figure (c), the particularly weak areas inside the dam are identified. These areas are located around x = 10-15 m and z = 3-6 m and x = 0-15 m and z =7-8 m.

5. CALCULATION OF LIQUEFACTION PROBABILITY

The effects of liquefaction damage on structures must be quantitatively clarified in order to establish the proper seismic design for structures. Liquefaction resistance factor F_L is used to evaluate liquefaction probability P_f. Liquefaction resistance factor F_L (Iwasaki et al., 1984) is calculated by the following equations:

$$F_L = \frac{R\left(N_{SPT}, F_c\right)}{L\left(a_{max}\right)} \tag{13}$$

$$F_L = F_L\left(x, z, a_{max}, N_{SPT}, F_c\right) = R\left(x, z, N_{SPT}, F_c\right) / L\left(z, a_{max}\right) \tag{14}$$

where R is the liquefaction resistance and L is the dynamic load. The emprical equations to calculate F_L are shown in Japan Road Association (2012) in detail. The relationship between factor F_L and P_f is given based on many in-situ investigations (Iwasaki et al., 1984), as shown in Fig. 9. The Iwasaki's relationship is utilized to transform F_L into P_f by function g, as shown in Eq. (15).

$$P_f\left(x, z, a_{max}\right) = g\left(F_L\right) = g\left(x, z, a_{max} N_{SPT}, F_c\right) \tag{15}$$

for which function g is given in Fig 9. In the numerical analysis, function g is introduced as a digital value.

In the analysis, random variables generated from the conditional simulation tool SGSIM, which uses the Ordinary Kriging theory and is included in GSLIB (Deutsch and Journel, 1992), are assigned to N_{SPT} and F_c. In this research, the conditional simulation "SGSIM" is used, since the evaluation of the liquefaction probability includes a complicated process. Since the Monte Carlo method is repeated 2000 times in the analysis, the expected value for liquefaction probability P_{fE} as the fragility is obtained at the grid points of the analyzed cross section by the following equation. Herein, the fragility means the liquefaction probability over the next 50 years as corresponds to a_{max}.

$$P_{fE}\left(x, z, a_{max}\right) = E\left\{g\left[F_L\left(x, z, a_{max}, N_{SPT}, F_c\right)\right]\right\} \tag{16}$$

Considering all the probabilistic variables, namely, N_{SPT}, F_c, and the peak ground acceleration of the dam over the next 50 years, a_{max}, the liquefaction probability over the next 50 years is calculated by Eq. (17) at the output points of the simulation (x, z) inside the dam.

$$P_{fE50}\left(x, z\right) = -\int_0^{\infty} \frac{dH\left(a_{max}\right)}{da_{max}} \cdot P_{fE}\left(x, z, a_{max}\right) da_{max} \tag{17}$$

where P_{fE50} is the liquefaction probability over the next 50 years at (x, z) inside the dam and H is the seismic hazard curve over the next 50 years at the top of the dam, as shown in Fig. 10.

To compare the degree of vulnerability against liquefaction among many dams all over Japan, the spatial average of P_{fE} and P_{fE50} of a dam could be useful. This is because the local liquefaction is difficult to compare quantitatively. The spatial average of P_{fE} is obtained for evaluating the fragility of the whole dam by Eq. (18).

$$\overline{P}_{fE}\left(a_{max}\right) = \frac{1}{L_x} \int_{L_x} \frac{\int_0^{20} P_{fE}\left(x, z, a_{max}\right)\left(10 - 0.5z\right) dz}{\int_0^{20} \left(10 - 0.5z\right) dz} dx \tag{18}$$

$\overline{P}_{fE}$ is the spatial average of the expected value for the liquefaction probability of the whole dam, and L_x is the horizontal length of the site investigation at the studied site, namely, 28 m. It is reasonable that the effect of liquefaction near the surface is more important than that in deeper areas. Therefore, P_{fE} is weighed based on the linear function of the depth direction. The

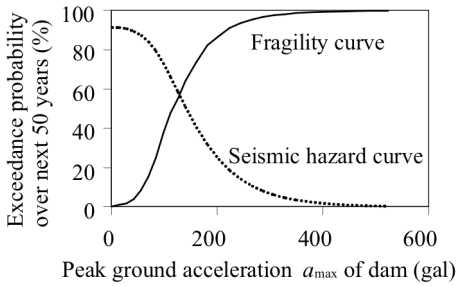

Figure 3. Seismic hazard curve and fragility curve of dam.

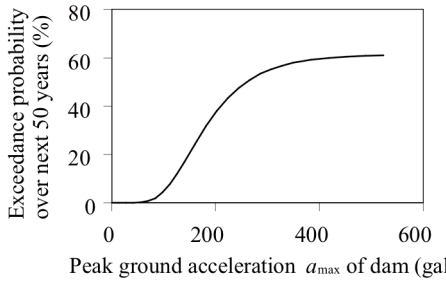

Figure 12. Cumulative distribution function of spatial average of liquefaction probability of dam over next 50 years $\overline{P}_{fE50}$.

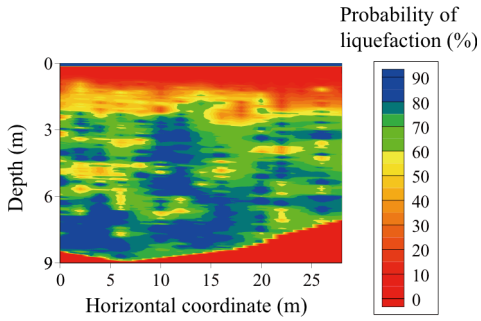

Figure 13. Spatial distribution of expected value of liquefaction probability when a_{max} equivalent to 140 gal.

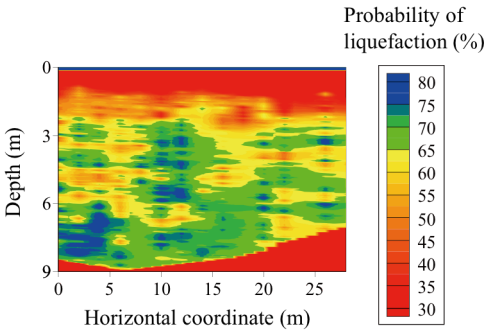

Figure 14. Spatial distribution of expected value of liquefaction probability over next 50 years.

weight decreases in the direction of depth and corresponds to 0 at z=20 m. This assumption is determined based on the results of the site investigations shown in Iwasaki et al. (1984).

The spatial average of P_{fE50} is calculated with the following equation:

$$\overline{P}_{fE50} = -\int_0^{\infty} \frac{dH(a_{max})}{da_{max}} \cdot \overline{P}_{fE}(a_{max}) da_{max} \quad (19)$$

where $\overline{P}_{fE50}$ is the liquefaction probability of the whole dam over the next 50 years.

6. EVALUATION OF LIQUEFACTION PROBABILITY OVER NEXT 50 YEARS

In Figure 11, the seismic hazard curve at the crest of the dam, shown in Fig. 10, and the fragility curve of the whole dam, calculated by Eq. (18), are summarized. The seismic hazard shown in Fig. 11 is relatively sensitive to the span of a_{max} from 111 to 223 gal. In addition, the fragility is relatively sensitive to the span of a_{max} from 70 to 203 gal. For a_{max} greater than 265 gal, the fragility becomes greater than 95%.

Fig. 12 shows the cumulative distribution function of the liquefaction probability of the whole dam over the next 50 years, $\overline{P}_{fE50}$, derived from Eq. (19). In the calculation of $\overline{P}_{fE50}$, the convolution integral of the seismic hazard, H, and the fragility curve, shown in Fig. 11, are employed. As a result, $\overline{P}_{fE50}$, which is the spatial average of the P_{fE50} of the dam, is evaluated as 61%. The value of the vertical axis in Fig. 12 shows the exceedance probability over the next 50 years; it increases about 32% between the peak ground acceleration, a_{max}, of 160 and 224 gal. It is derived from the condition whereby not only is the fragility high, but the probability of the occurrence of an earthquake is high in that range of a_{max}, as shown in Fig. 11. As $\overline{P}_{fE50}$ =61% is not small, the liquefaction probability of the dam against a Nankai Trough earthquake cannot be ignored.

Fig. 13 shows the spatial distribution of the expected value of the liquefaction probability when a_{max} is equivalent to 140 gal. The value of a_{max} =140 gal is predicted to be nearly 50% at the site over the next 50 years. N_{SPT} is relatively small at x = 0-16 m, z = 7-8 m and at x = 10-13 m, z = 3-6 m, as shown in Fig. 8(a). Corresponding to the tendency of N_{SPT}, the liquefaction probability in these areas is relatively high.

Fig. 14 shows the spatial distribution of P_{fE50} inside the dam calculated by Eq. (17). According to Fig. 14, the liquefaction probability over the next 50 years is relatively high at locations similar to those seen in Fig. 13. Based on the results shown in Figs. 13 and 14, it seems that the N_{SPT} values have a greater influence on the liquefaction probability.

The number of CPTUs used in this case is quite large; and therefore, the example presented here is exceptional. For real applications, the investigation costs should be considered in many cases. As for cost-effective approaches, the mixed approach of the soundings and geophysical surveys (e.g., Nishimura, et al., 2016) can be considered. As other practical concepts, the extension and utilization of the database for the statistical values of soil parameters (e.g., Ching and Phoon, 2019) can be mentioned. In Ching's approach, the information from the database is mixed and used with the values measured in-situ to characterize the soil properties of the site in question.

Since the CPTUs were conducted in short intervals for examining the spatial variability of N_{SPT}

and F_c, it was possible to evaluate in detail the location and the scale of the weak areas against the liquefaction inside the dam over the next 50 years. Based on the spatial distribution of the liquefaction probability, the diagnosis of an earth-fill dam against liquefaction is made properly. In addition, introducing the seismic hazard and the fragility curve into the calculation of the liquefaction probability of an earth-fill dam, the liquefaction hazard during the selected time period could be incorporated. Using the seismic hazard and the fragility curve of the dams, if the dams are located in different parts of Japan, the priority of the improvements to be made to them against the probable liquefaction damage of each dam can be compared based on the proposed method. Therefore, the proposed method for evaluating the liquefaction probability of an earth-fill dam can provide useful information for determining the order of priority among the many dams in Japan in terms of making improvements to them.

7. Conclusions

The spatial distribution of the liquefaction probability inside the studied dam has been calculated in detail from CPTUs including conversion errors and the spatial variability of the soil parameters. In addition, based on the seismic hazard at the studied site and the fragility of the dam, the spatial average of the liquefaction probability of the dam over the next 50 years has been evaluated. The concluding remarks are summarized below.

1. The conversion errors, from the CPTU N-value, N_c, to the SPT N-value, N_{SPT}, and from the fines content, F_{cIc}, obtained from I_c, to the proper fines content, F_c, have been quantified, respectively, in the conversion formulas proposed in this study. According to the results of a conditional simulation with the conversion errors, the standard deviation of F_c has been calculated as nearly 30% in the dominant area of the studied dam. The value seems large in comparison to the mean value.

2. The spatial structures of $\log N_c$ and $\log F_c$ have been determined based on the densely measured data from the CPTUs. Since the CPTUs were conducted with 2-m intervals in the horizontal direction, an extensive data set of F_c has been estimated from the CPTUs through the use of conversion formulas. As a result, the correlation distances of $\log N_c$ and $\log F_c$ have been reasonably identified, because the horizontal value was about 10 times that of the vertical one.

3. Utilizing the conditional simulation, the spatial distribution of the expected values for F_c and N_{SPT}, the standard deviation of F_c and N_{SPT}, and the probability that the simulated values inside the dam would be lower than the prescribed threshold values for F_c and N_{SPT}, respectively, have been visualized in detail. These results clarify the scale of the weak area and the spatial continuity of the soil profile inside the dam.

4. The seismic hazard at the studied site and the fragility against the liquefaction of the dam have been introduced into the evaluation of the liquefaction probability of the dam over the next 50 years. As a result, it has been confirmed that the spatial average of the liquefaction probability of the dam over the next 50 years has been calculated as 61%. Although the desired value of the liquefaction probability of a dam depends on the situation, the liquefaction probability of dams calculated by the proposed method can offer supporting evidence for decision-making in terms of improving the dams.

Nevertheless, dense data are required to identify the spatial structure of the soil parameters in order to evaluate the liquefaction probability of a dam, and the number of test data is not enough for the statistical modeling. Therefore, to calculate the liquefaction probability with limited information, a database for the spatial structure of the soil parameters needs to be developed. Although the data obtained from the SPT or laboratory tests are generally sparse for characterizing the statistical model, an extensive data set on the soil parameters can be obtained by applying conversion formulas to the measured data from CPTUs. Thus, the proposed method could be useful for evaluating the spatial structure of the soil parameters properly and for developing a database for the spatial structure of the soil parameters.

A common problem for evaluating the liquefaction probability of an earth-fill dam is the limited time and the limited budget for site investigations. It has been shown that the proposed method can accurately evaluate the liquefaction probability of a dam based on the N-value and F_c; and thus, the accumulated soil data from past site investigations, such as the SPT N-value and F_c, can be easily introduced into the proposed method. Several methods to synthesize the different sources of the investigation data have been proposed (e.g., Nishimura et al., 2016; Cardarelli et al., 2014), and their applicability to the evaluation of the liquefaction probability should be studied.

Acknowledgement

The project presented in this article is supported by Grant‐in‐Aid for Scientific Research (A), Grant Numbers 26252040 and 16H02577, of the Japanese Society for the Promotion of Science (JSPS).

References

[1] Tatsuoka, F., Koseki, J., Takahashi, A. "Earthquake-induced damage to earth structures and proposal for revision of their design policy -based on a case history of the 2011 off the Pacific coast of Tohoku Earthquake-", Journal of Japan Society of Civil Engineering, Volume(5), pp. 101–112, 2017. https://doi.org/10.2208/journalofjsce.5.1_101

[2] Ono, K., Kazama, S., Kawagoe, S., Yokoo, Y., Gunawardhana, L. "Possible earthen dam failure mechanisms of Fujinuma reservoir due to the Great East Japan Earthquake of 2011", Hydrological Research Letters, Volume(5), pp. 69–72, 2011. https://doi.org/10.3178/hrl.5.69

[3] Ministry of Agriculture Forestry and Fisheries "The Design Guideline of Land Improvement Project (Improvement of an Earth-Fill Dam)", Japanese Society of Irrigation, Drainage and Rural Engineering, Toyo, 2015, (In Japanese).

[4] Iwasaki, T., Arakawa, T., Tokida, K. "Simplified Procedures for Assesing Soil Liquefaction During Earthquakes", Soil Dynamics and Earthquake Engineering, Volume(3), pp. 49–58, 1984.

[5] Robertson, P.K., Wride, C.E. "Evaluating Cyclic Liquefaction Potential Using the CPT", Canadian Journal of Geotechnical Engineering, Volume(35), pp. 442–459, 1998.

[6] Suzuki, Y., Tokimatsu, K., Sanematsu, T. "Correlations between CPT data and soil characteristics obtained from SPT", Journal of

Structural and Construction Engineering, Volume(566), pp. 73-80, 2003, (In Japanese). https://doi.org/10.3130/aijs.68.73_2
[7] Robertson, P.K. "Soil classification using the cone penetration test", Canadian Journal of Geotechnical Engineering, Volume(27), 151–158, 1990. https://doi.org/10.1139/t90-014
[8] Journel, A.G., Huijbregts, C.J. "Mining geostatistics", Academic Press, London, United Kingdom, 1978.
[9] Vanmarcke, E. "Random Fields: Analysis and Synthesis", MIT Press, Cambridge, USA, 1983.
[10] Phoon, K.-K., Kulhawy, F.H. "Characterization of geotechnical variability", Canadian Journal of Geotechnical Engineering, Volume(36), pp. 612–624, 1999. https://doi.org/10.1139/t99-038
[11] Nishimura, S., Shibata, T., Shuku, T. "Diagnosis of earth-fill dams by synthesised approach of sounding and surface wave method", Georisk, Volume(10), pp. 312–319, 2016. https://doi.org/10.1080/17499518.2016.1197406
[12] Akaike, H. "A New Look at the Statistical Model Identification", IEEE Transactions on Automatic Control, Volume(19), pp. 716–723, 1974. https://doi.org/10.1109/TAC.1974.1100705
[13] Nishimura, S. "The investigation of the establishment method of soil parameters", Proceedings of Symposium of Performance Design and Deformation Prediction of Geotechnical Structure During Earthquake, pp. 121–126, 2007.
[14] Deutsch, C. V, Journel, A.G. "Geostatistical Software Library and User's Guide", Oxford University Press, Oxford, England, 1992.
[15] Imaide, K., Nishimura, S., Shibata, T., Shuku, T. "Evaluation of the spatial variability of cone penetration resistance inside an earth-fill dam composed of materials with different particle size distribution", Journal of Japan Society of Civil Engineering, Series C (Geosphere Engineering), Volume(74), pp. 213–224, 2018, (In Japanese). https://doi.org/10.2208/jscejge.74.213
[16] Imaide, K., Nishimura, S., Shibata, T., Shuku, T. "Evaluation of the Spatial Variability of Cone Penetration Resistance Inside an Earth-Fill Dam Composed of Materials with Different Particle Sizes with Use of Geostatistics", 16th Asian Regional Conference on Soil Mechanics and Geotechnical Engineering, Taipei, Taiwan, October 14-18, 2019.
[17] Japan Road Association "Specification for highway bridge, Part 5 Seismic Design", Maruzen, Tokyo, 2012, (In Japanese).
[18] Ching, J., Phoon, K.-K. "Constructing Site-Specific Multivariate Probability Distribution Model Using Bayesian Machine Learning", Journal of Engineering Mechanics, Volume(145), 4018126, 2019. https://doi.org/10.1061/(ASCE)EM.1943-7889.0001537
[19] Cardarelli, E., Cercato, M., De Donno, G. "Characterization of an earth-filled dam through the combined use of electrical resistivity tomography, P- and SH-wave seismic tomography and surface wave data", Journal of Applied Geophysics, Volume(106), pp. 87–95, 2014. https://doi.org/https://doi.org/10.1016/j.jappgeo.2014.04.007